

Response to Editor's minor revisions

We thank the Editor for pointing out the presence of typos and mistakes in the manuscript. We corrected the typos and additionally applied the following changes:

Line 131: This sentence was difficult to read and it was shortened as the reference information for each dataset is clearly specified in both Fig. 3 and 4.

Line 145: “assuming” changed in “on the assumption that”

Line 307: Rephrased into

“the statistical deviation of the slopes of H2 and I2 is clearer when comparing them with the average slope calculated for all the events at each site, since the slopes of H2 and I2 fall outside the (99.99%) confidence limits (Fig. 7).”

Line 626: The figure caption for Fig. 2 was shortened.

1 **Frequency, magnitude and character of hyperthermal**
2 **events at the onset of the Early Eocene Climatic**
3 **Optimum**

4 **V. Lauretano¹, K. Littler^{2,*}, M. Polling¹, J. C. Zachos², L. J. Lourens¹**

5 [1]{Department of Earth Sciences, Faculty of Geosciences, Utrecht University,
6 Budapestlaan 4, 3584CD, Utrecht, The Netherlands}

7 [2]{Department of Earth and Planetary Sciences, University of California Santa Cruz,
8 1156 High Street, Santa Cruz, CA 95064, USA}

9 [*]{now at: Camborne School of Mines, University of Exeter, Penryn Campus,
10 Penryn, Cornwall, TR10 9FE, United Kingdom}

11 Correspondence to: Vittoria Lauretano (v.lauretano@uu.nl)

12

13 **Abstract**

14 Recent studies have shown that the Early Eocene Climatic Optimum (EECO) was
15 preceded by a series of short-lived global warming events, known as hyperthermals.
16 Here we present high-resolution benthic stable carbon and oxygen isotope records
17 from ODP Sites 1262 and 1263 (Walvis Ridge, SE Atlantic) between ~54 and ~52
18 million years ago, tightly constraining the character, timing, and magnitude of six
19 prominent hyperthermal events. These events, **which** include Eocene Thermal
20 Maximum (ETM) 2 and 3, are studied in relation to orbital forcing and long-term
21 trends. Our findings reveal an almost linear relationship between $\delta^{13}\text{C}$ and $\delta^{18}\text{O}$ for all
22 these hyperthermals, indicating that the eccentricity-paced co-variance between deep-
23 sea temperature changes and extreme perturbations in the exogenic carbon pool
24 persisted during these events towards the onset of the EECO, in accord with previous
25 observations for the Paleocene Eocene Thermal Maximum (PETM) and ETM2. The
26 covariance of $\delta^{13}\text{C}$ and $\delta^{18}\text{O}$ during H2 and I2, which are the second pulses of the
27 “paired” hyperthermal events ETM2-H2 and I1-I2, deviates with respect to the other
28 events. We hypothesize that this could relate to a relatively higher contribution of an

Vittoria 17/9/2015 10:46

Deleted: that

30 isotopically heavier source of carbon, such as peat or permafrost, and/or to climate
31 feedbacks/local changes in circulation. Finally, the $\delta^{18}\text{O}$ records of the two sites show
32 a systematic offset with on average 0.2‰ heavier values for the shallower Site 1263,
33 which we link to a slightly heavier isotopic composition of the intermediate water
34 mass reaching the northeastern flank of the Walvis Ridge compared to that of the
35 deeper northwestern water mass at Site 1262.

Lauretano, V. (Vittoria) 16/9/2015 11:36
Deleted: e

37 1 Introduction

38 The early Paleogene was characterized by a highly dynamic climatic system both on
39 long- ($>10^6$ years) and short- ($<10^4$ years) time scales. From the late Paleocene (~58
40 Ma) to the early Eocene (~50 Ma), Earth's surface experienced a long-term warming
41 trend that culminated in an extended period of extreme warmth, called the Early
42 Eocene Climatic Optimum (EECO; Zachos et al., 2001, 2008; Bijl et al., 2009;
43 Westerhold and Röhl, 2009). During the EECO, global temperatures reached a long-
44 term maximum lasting about 2 Myr, characterized by the warmest temperatures of the
45 Cenozoic (Zachos et al., 2008). Superimposed on the long-term warming trend were a
46 series of short-lived global warming (hyperthermal) events, accompanied by the
47 release of ^{13}C -depleted carbon into the ocean-atmosphere carbon reservoirs (Zachos et
48 al., 2005; Lourens et al., 2005; Nicolo et al., 2007; Littler et al., 2014; Kirtland Turner
49 et al., 2014). These events are of particular interest as they represent useful analogs
50 for the current global warming, despite differences in background climatic conditions
51 and rates of change (e.g., Zachos et al., 2008; Hönisch et al., 2012; Zeebe and Zachos,
52 2013).

Lauretano, V. (Vittoria) 16/9/2015 11:55
Deleted: , Ma

Lauretano, V. (Vittoria) 16/9/2015 11:56
Deleted: s

Unknown
Field Code Changed

53 The Paleocene Eocene Thermal Maximum (PETM or ETM1, ~56 Ma), lasting less
54 than 200 kyr, was the most extreme of these episodes. During the PETM global
55 temperature rose by 5–8°C, and massive amounts of carbon were released as
56 evidenced by a significant negative carbon isotope excursion (CIE) of $>3\%$ in the
57 ocean/atmosphere carbon pools, and widespread dissolution of seafloor carbonate
58 (Kennett and Stott, 1991; Dickens et al., 1995; Thomas and Shackleton, 1996; Zachos
59 et al., 2005; Sluijs et al., 2007; Zachos et al., 2008; McInerney and Wing, 2011). A
60 series of similar events are recorded in carbonate records from marine and continental
61 deposits from the early Paleogene, as expressed by negative excursions in $\delta^{13}\text{C}$ and
62 $\delta^{18}\text{O}$ often accompanied by dissolution horizons (e.g., Cramer et al., 2003; Lourens et

Unknown
Field Code Changed

66 al., 2005; Agnini et al., 2009; Galeotti et al., 2010; Stap et al., 2010; Zachos et al.,
67 2010; Abels et al., 2012; Slotnick et al., 2012; Kirtland Turner et al., 2014; Littler et
68 al., 2014; Abels et al., 2015). Orbitally tuned records for this geological interval
69 provide evidence that the early Eocene hyperthermal events were paced by variations
70 | in the Earth's orbit, specifically in the long- and short- eccentricity cycles. (e.g.,
71 Cramer et al., 2003; Lourens et al., 2005; Littler et al., 2014; Zachos et al., 2010;
72 Sexton et al., 2011).

73 Several different carbon sources have been proposed to explain the negative CIE,
74 including: (1) the release of methane by thermal dissociation of gas hydrates on the
75 continental slopes (Dickens et al., 1995); (2) the burning of peat and coal deposits
76 (Kurtz et al., 2003); and (3) the release of carbon from thawing of permafrost soils at
77 | high latitudes as a feedback or as a direct response to orbital forcing (DeConto et al.,
78 2012); while (4) a redistribution of ^{13}C -depleted carbon within oceans has been
79 proposed as mechanism for hyperthermals in the early to middle Eocene interval
80 (Sexton et al., 2011).

81 Despite the uncertainty in carbon source and triggering mechanism of the
82 hyperthermal events, a common reservoir has been theorized to explain the consistent
83 covariance in benthic foraminiferal $\delta^{13}\text{C}$ and $\delta^{18}\text{O}$ across both the PETM and ETM2,
84 indicating that changes in the exogenic carbon pool were similarly related to warming
85 during these events (Stap et al., 2010). The aim of this paper is to test this relationship
86 by constraining the relative timing and magnitude of changes in deep ocean
87 temperatures and carbon isotope excursions for a series of carbon isotope excursions
88 that succeed ETM2, initially identified by Cramer et al., (2003) in the composite bulk
89 carbonate $\delta^{13}\text{C}$ record from several deep-sea sites (ODP Sites 690 and 1051; DSDP
90 Site 550 and 577). For this purpose, we generated high-resolution carbon and oxygen
91 stable isotope records of the benthic foraminiferal species *Nuttalides truempyi* from
92 ODP Sites 1262 and 1263 (Walvis Ridge) encompassing the interval from the ETM2
93 | (Stap et al., 2010) to the ETM3 (Röhl et al., 2005), providing the first complete high-
94 resolution benthic stable isotope records for the early Eocene events leading to the
95 onset of the EECO.

96

Lauretano, V. (Vittoria) 16/9/2015 12:03
Deleted: Deconto

98 2 Materials and Methods

99 2.1 Site location and sampling

100 ODP Sites 1262 and 1263 represent the deepest and shallowest end-members of a 2-
101 km depth transect recovered during ODP Leg 208. Site 1263 is located just below the
102 crest of the northeast flank of Walvis Ridge, in the southeastern Atlantic, at a water
103 depth of 2717 m, whereas Site 1262 was drilled near the base of the northwestern
104 flank of Walvis Ridge at a water depth of 4759 m (Fig. 1). The estimated paleodepths
105 of Sites 1262 and 1263 at ~56 Ma were ~3600 m and 1500 m, respectively (Zachos et
106 al., 2004). The material recovered at the two sites provided an expanded sequence of
107 early Paleogene sediments, yielding a complete section mainly composed of
108 calcareous nannofossil ooze, chalk and marls. The composite depth scale for Site
109 1263 was constructed using the magnetic susceptibility (MS) and sediment lightness
110 (L*) from the four holes (Zachos et al., 2004).

111 Samples were collected at the Bremen Core Repository from Holes A, B and C for
112 Site 1263, and Holes A and B for Site 1262, according to the shipboard meters
113 composite depth section (mcd) (Zachos et al., 2004). A 28-m thick interval of Site
114 1263 was sampled at a resolution of 5 cm from ~268 to ~296 mcd, and a ~6-m
115 interval of Site 1262 was sampled at a resolution of 3 cm from ~103 to ~109 mcd
116 (Fig. 3). Prior to the analyses, samples were freeze dried, washed and sieved to obtain
117 fractions larger than 38, 63 and 150 μm at University of California, Santa Cruz and
118 Utrecht University.

119

120 2.2 Stable isotopes

121 Multi-specimen samples of *N. truempyi* were picked from the >150 μm fraction. The
122 stable isotope values of picked specimens (average of 6–8 foraminiferal calcite tests)
123 from Site 1263 were carried out at Utrecht University using a CARBO-KIEL
124 automated carbonate preparation device linked on-line to a Thermo-Finnigan
125 MAT253 mass spectrometer. Calibrations to the international standard (NBS-19) and
126 to the in-house standard (Naxos marble) show an analytical precision of 0.03‰ and
127 0.08‰ for $\delta^{13}\text{C}$ and $\delta^{18}\text{O}$, respectively. The stable isotope values of picked specimens

128 from Site 1262 were analyzed on a KIEL IV carbonate preparation device linked on-
 129 line to a Thermo-Finnigan MAT253 mass spectrometer, at the UCSC Stable Isotope
 130 Laboratory, Santa Cruz. Calibrations to the in-house standard Carrara marble (CM05)
 131 and international standards (NBS-18 and NBS-19) yield an analytical precision of
 132 0.05‰ and 0.08‰, for $\delta^{13}\text{C}$ and $\delta^{18}\text{O}$, respectively. All values are reported in
 133 standard delta notation relative to VPDB (Vienna Pee Dee Belemnite). Outliers were
 134 defined by adding or subtracting an upper and lower boundary of 2σ from a 13-points
 135 moving average, following the method by Liebrand et al. (2011). Published benthic
 136 isotope data of the same foraminiferal species were included in this study to obtain
 137 longer continuous records of Site 1263 and 1262 (Stap et al., 2010; Littler et al.,
 138 2014), (Fig. 3 and 4).

139 2.3 Paleotemperature reconstructions

140 Paleotemperatures were obtained from the benthic foraminiferal $\delta^{18}\text{O}$ values by
 141 applying the equation of Bemis et al. (1998):

$$142 \quad T_{\text{C}} = 16.9 - 4.38 (\delta^{18}\text{O}_{\text{c}} - \delta^{18}\text{O}_{\text{sw}}) + 0.10 (\delta^{18}\text{O}_{\text{c}} - \delta^{18}\text{O}_{\text{sw}})^2 \quad (1)$$

143 The temperature scale is computed assuming an ice-free sea water value ($\delta^{18}\text{O}_{\text{sw}}$) of -
 144 1.2‰ (VPDB). This value is calculated correcting the estimated deep-sea $\delta^{18}\text{O}_{\text{sw}}$
 145 value of -0.98‰ (SMOW) relative to PDB scales by subtracting 0.27‰ (Hut, 1987).
 146 The *N. truempyi* $\delta^{18}\text{O}$ was adjusted for disequilibrium vital effects by adding 0.35‰
 147 (Shackleton et al., 1984; Shackleton and Hall, 1997), on the assumption that the
 148 isotopic disequilibrium for this species remained constant through time.

149 3 Age model

151 Given the typical low resolution age control afforded by magneto- and bio-
 152 stratigraphy, and the availability of a robust cycle (i.e., orbital) based chronology for
 153 the Leg 208 sites (Westerhold et al., 2007), we developed an eccentricity-tuned age
 154 model for the studied interval using the red over green color ratio (a^*) records of ODP
 155 Sites 1263 and 1262 (Fig. 2). For tuning, we applied first spectral analysis in the
 156 depth domain using standard Blackman-Tukey and Gaussian filtering techniques as
 157 provided by the AnalySeries program (Paillard et al., 1996). Site 1262, the deepest
 158 site at Walvis Ridge, was chosen as the backbone for our tuning. The a^* record of this

Vittoria 17/9/2015 11:13
 Deleted: for the ETM2 (or H1/Elmo event) and H2

Lauretano, V. (Vittoria) 16/9/2015 13:42
 Deleted: a

Vittoria 17/9/2015 11:14
 Deleted:)

Vittoria 17/9/2015 11:13
 Deleted: and for I1ETM2 (Stap et al., 2010) and H2 to -I2

Vittoria 17/9/2015 11:13
 Deleted: of Site 1262

Vittoria 17/9/2015 11:14
 Deleted: (

Lauretano, V. (Vittoria) 16/9/2015 13:54
 Deleted: .

Lauretano, V. (Vittoria) 16/9/2015 13:56
 Deleted: ($\delta^{18}\text{O}_{\text{sw}}$)

Lauretano, V. (Vittoria) 16/9/2015 13:56
 Deleted:

Lauretano, V. (Vittoria) 16/9/2015 13:56
 Deleted: deep

Lauretano, V. (Vittoria) 16/9/2015 13:58
 Deleted: ing

172 site clearly revealed a ~3-m period, interpreted as reflecting the climatic imprint of the
173 405-kyr eccentricity cycle (Lourens et al., 2005). Subsequently, we filtered this
174 component and tuned it directly to the extracted 405-kyr eccentricity component of
175 the La2010d orbital solution (Laskar et al., 2011) with maximum a^* values,
176 interpreted to represent maximum carbonate dissolution, corresponding to maximum
177 eccentricity values (Table 1). A similar approach was carried out for the a^* record of
178 Site 1263 to evaluate the continuity of the successions and robustness of the filtered
179 output (Fig. 2). Finally, the tuned age model of Site 1262 was transferred to Site 1263
180 by correlating >50 characteristic features in the a^* records of both sites as tie points
181 (Fig.2 and Table 2).

182 Different tuning options have been debated in the last 10 years, resulting in an age for
183 the PETM ranging between ~55.5 and ~56.3 Ma (Lourens et al., 2005; Westerhold et
184 al., 2008; Hilgen et al., 2010, Dinarès-Turell et al., 2014). Here we report on two
185 tuning options (Fig. 2), assigning an age of 53.69 ± 0.02 Ma (option 1) or of
186 54.09 ± 0.02 Ma (option 2) to ETM2 (Westerhold et al., 2007). According to both
187 options, ETM2 predates the 405-kyr maximum falling at an increasing limb, in
188 agreement with observations of Westerhold et al. (2007), but in contrast with the
189 earlier interpretation by Lourens et al. (2005), who aligned this event to a maximum
190 in the 405-kyr cycle. Recent literature revising the Paleocene cyclostratigraphic
191 interpretation (Dinarès-Turell et al., 2014; Hilgen et al., 2015) have shown that the
192 Paleocene holds 25, rather than 24, 405-kyr eccentricity cycles. In addition, new U/Pb
193 ages have become available which support an age of ~66.0 Ma for the K/Pg boundary
194 (Kuiper et al., 2008; Renne et al., 2013). These developments point to an age of ~54.0
195 Ma for ETM2 and therefore we plot our results anchoring the age of ETM2 to option
196 2 (Fig. 4). Evolutionary wavelet spectra were obtained in the time domain using the
197 wavelet script of Torrence and Compo (<http://paos.colorado.edu/research/wavelets>).
198 Prior to the analysis, carbon and oxygen records were resampled at 2.5 kyrs,
199 detrended and normalized.

200

201 4 Results

202 Our new benthic $\delta^{13}C$ and $\delta^{18}O$ records show six major negative excursions between
203 54 and 52 Ma (Fig. 4). They correspond to the ETM2, H2, I1, I2, J, and ETM3 (or
204 X/K) events, formerly recognized in deep-sea $\delta^{13}C$ bulk carbonate records and land-

Lauretano, V. (Vittoria) 16/9/2015 15:10

Deleted: My

Lauretano, V. (Vittoria) 16/9/2015 15:15

Deleted: /

207 based marine and continental sections (Abels et al., 2012; Agnini et al., 2009; Cramer
208 et al., 2003; Kirtland Turner et al., 2014; Littler et al., 2014; Lourens et al., 2005;
209 Slotnick et al., 2012; Abels et al., 2015).

210 The general long-term trend in our ~2-Myr long records indicates a minor increase
211 between 54.2 Ma and 53.2 Ma followed by an average decrease of ~0.3 ‰ in absolute
212 baseline values of both $\delta^{13}\text{C}$ and $\delta^{18}\text{O}$ following J (~53.1 Ma), accompanied by minor
213 cycles between the six main events in both records. Following J, both records
214 maintain rather stable values up to ETM3 (Fig. 4). These changes are negligible
215 compared to the Paleocene-Eocene long-term warming trend and long-term negative
216 trend in carbon isotope values. However, the onset of more generally negative $\delta^{13}\text{C}$
217 values, coinciding with J, has also been observed in the deep-sea bulk carbonate
218 record at Site 1262 (Zachos et al., 2010) and in the land-based section at Mead Stream
219 by Slotnick et al. (2012), who suggested that the pronounced change in lithology
220 beginning with J could be used as a chronostratigraphic marker for the onset of the
221 EECO.

222 Evidence for the onset of warmer temperatures leading to the EECO is evident at ~53
223 Ma in the benthic $\delta^{18}\text{O}$ records at both Sites 1262 and 1263 (Fig. 4). Baseline average
224 $\delta^{18}\text{O}$ values prior to ETM2, signifying the response of the unperturbed oceanic
225 system, indicate a mean deep-sea temperature of ~12°C, which post-J increases by
226 >0.5°C. Despite variability, our data shows that this increase in background
227 temperature continued upwards across ETM3. Here we suggest that the onset of the
228 EECO can be identified in our records with the onset of the general low in benthic
229 isotope values initiated with J (~53 Ma) and thus including ETM3 within the EECO.
230 Although longer high-resolution benthic $\delta^{18}\text{O}$ records are needed to establish the total
231 duration of the EECO, this could represent a first step towards a formal definition of
232 the warmest interval of the Cenozoic, avoiding ambiguity caused by changes in the
233 time scale.

234 On the short-term scale, our new data across the events following ETM2 and H2
235 indicate a rise in temperature of ~2 °C and ~1.5 °C during I1 and I2, respectively. The
236 J-event was associated with a temperature increase of >1°C superimposed on the
237 further average decrease in baseline $\delta^{18}\text{O}$ value. ETM3 is expressed in both the
238 shallowest and deepest site at Walvis Ridge by similar isotopic excursions, with a CIE

Lauretano, V. (Vittoria) 16/9/2015 15:16
Deleted: 2

Lauretano, V. (Vittoria) 16/9/2015 15:17
Deleted: baseline values

Lauretano, V. (Vittoria) 16/9/2015 15:17
Deleted: with

Lauretano, V. (Vittoria) 16/9/2015 15:18
Deleted: evident

Lauretano, V. (Vittoria) 16/9/2015 15:21
Deleted: represent

Lauretano, V. (Vittoria) 16/9/2015 15:32
Deleted: The

245 of $\sim 0.8\%$ and a negative shift in the $\delta^{18}\text{O}$ record of $\sim 0.5\%$, corresponding to a
246 warming in the deep ocean of $2\text{--}2.5^\circ\text{C}$, comparable to values observed during the
247 ETM2 (Stap et al., 2010).

248 Evolutionary wavelet analyses for $\delta^{13}\text{C}$ and $\delta^{18}\text{O}$ records of Site 1263 show spectral
249 power concentrated at distinct frequencies, corresponding to the long 405-kyr and
250 short $\sim 100\text{-kyr}$ eccentricity cycles (Fig. 5). The isotope records reveal coherent
251 patterns, with the highest spectral power concentrated during ETM2-H2 and I1-I2.
252 The $\sim 100\text{-kyr}$ signal in $\delta^{13}\text{C}$, which is very prominent in the first 1 Myr of the record,
253 weakens after J. The imprint of precession and/or obliquity forcing is very
254 weak/absent throughout the entire record. As a result of our tuning approach, minima
255 in $\delta^{13}\text{C}$ are approximately in phase with maxima in the 405-kyr and $\sim 100\text{-kyr}$
256 eccentricity cycles, following previous work (e.g., Cramer et al., 2003; Lourens et al.,
257 2005; Zachos et al., 2010; Stap et al., 2010).

258 5 Discussion

259 5.1 Isotope covariance

260 Our high-resolution benthic isotope records provide a direct constraint on the
261 relationship between the temperature-related signal carried by the benthic
262 foraminiferal $\delta^{18}\text{O}$ and the CIEs during the events leading to the EECO. The six
263 events recognised in the benthic records vary in terms of both magnitude of the CIEs
264 and inferred temperature changes. The most intense perturbations are associated with
265 ETM2, I1 and ETM3, whereas H2 and I2, which lag the larger events by one 100-kyr
266 eccentricity cycle, are less prominent (Fig. 4). One important question then is whether
267 all these events of varying magnitude are accompanied by the same source of light
268 carbon released into the ocean atmosphere system and climatic response. Following
269 Stap et al. (2010), we have assessed this by comparing the slopes of the regression
270 lines between the carbon and oxygen isotopes of the individual events (Fig. 6). These
271 cross-plots clearly show that all events exhibit significant and coherent linear
272 correlation at both sites with slopes ranging between 0.5 and 0.7 (Fig. 6), indicating a
273 consistent relationship for all events between changes in deep-sea temperatures and
274 carbon release. We conclude that this significant covariance between benthic $\delta^{13}\text{C}$ and
275 $\delta^{18}\text{O}$ records suggests a strong non-linear response to orbital forcing of global
276 temperatures and the release of isotopically light carbon (e.g. methane gas and/or

Lauretano, V. (Vittoria) 16/9/2015 15:33

Deleted: the

Lauretano, V. (Vittoria) 16/9/2015 15:44

Deleted: the

Lauretano, V. (Vittoria) 16/9/2015 15:44

Deleted: the

Lauretano, V. (Vittoria) 16/9/2015 15:36

Deleted: the

Lauretano, V. (Vittoria) 16/9/2015 15:45

Deleted: in

Lauretano, V. (Vittoria) 16/9/2015 15:46

Deleted: g

Lauretano, V. (Vittoria) 16/9/2015 16:49

Deleted: -7

Lauretano, V. (Vittoria) 16/9/2015 15:47

Deleted: the

285 CO₂) into the ocean-atmosphere system during eccentricity maxima, driving
286 subsequent carbonate dissolution and enhanced greenhouse warming, as has been
287 observed in the older part of the record at Site 1262 (Stap et al., 2010; Littler et al.,
288 2014). This conclusion is further underlined by the consistent scaling of CIE
289 magnitudes between our deep-sea data and soil nodule records of the Bighorn basin
290 for these events, which strengthens the hypothesis of a similar isotopic composition of
291 the carbon source for the early Eocene hyperthermal events (Abels et al., 2015).

292

293 5.2 The “paired” hyperthermal events

294 The slopes of the regression lines for H2 and I2 appear slightly steeper than those of
295 ETM2, I1, J and ETM3 (Fig. 6). To statistically test this (dis)similarity, we applied a
296 Student t-test to pairs of slopes, comparing all the events against each other using both
297 a pooled and an unpooled error variance. The results show that the null hypothesis
298 (the slopes being similar, $\alpha=0.05$) is satisfied in the case of ETM2, I1, J and ETM3.
299 The tests on the steeper slopes of H2 and I2 generally display values of $p \leq 0.05$ when
300 tested against the other events, but values of $p \geq 0.05$ when tested against each other.
301 This implies that the smaller events, H2 and I2, are statistically similar to each other
302 but differ slightly from the other perturbations. Even though this statistical approach
303 might be subject to limitations derived from the range of data points chosen for each
304 event, it clearly shows that the slopes for H2 and I2 deviate from the average values
305 given by the other events. Moreover, the statistical deviation of the slopes of H2 and
306 I2 is clearer when comparing them with the average slope calculated for all the events
307 at each site, since the slopes of H2 and I2 fall outside the (99.99%) confidence limits
308 (Fig. 7). The average slope between $\delta^{13}\text{C}$ and $\delta^{18}\text{O}$ of 0.6 for both sites is also in
309 accord with previous observations for the onset/recovery of PETM, ETM2 and H2 by
310 Stap et al. (2010).

311 The “paired” hyperthermal events, ETM2-H2 and I1-I2 thus reveal slightly different
312 $\delta^{13}\text{C}$ vs. $\delta^{18}\text{O}$ relationships between their first (ETM2 and I1) and secondary (H2 and
313 I2) pulses. Assuming that these signals are globally representative, this could imply
314 that the second of the two pulses had a relatively larger contribution of an isotopically
315 heavier carbon source than the first pulse. Such a mechanism could hint to a methane-
316 related dominant carbon source (e.g. methane hydrates) during the initial phase of the
317 paired hyperthermal events that is mostly depleted, so that other relatively heavier

Lauretano, V. (Vittoria) 16/9/2015 15:54

Deleted: of the

Lauretano, V. (Vittoria) 16/9/2015 15:54

Deleted: two s

Lauretano, V. (Vittoria) 16/9/2015 15:54

Deleted: s

Lauretano, V. (Vittoria) 16/9/2015 15:55

Deleted: they

322 carbon isotope sources (e.g. wetlands, peat) become progressively more important
323 during the successive event. Warming of intermediate water during ETM2 and I1, as
324 previously suggested for the PETM and ETM2 (Jennions et al., 2015; Lunt et al.,
325 2010), could have destabilized methane clathrates leading to their dissociation and the
326 subsequent increased warming and large CIE. Mechanisms related to the depletion
327 and subsequent recharge time of the inferred methane clathrate reservoir between
328 ETM2 and H2, and I1 and I2, could explain why the second event had both a smaller
329 magnitude and possibly a smaller relative contribution of methanogenic carbon. The
330 smaller magnitude of the two secondary carbon pulses, regardless of the isotopic
331 composition of their source, seems feasible because the a^* values, interpreted as
332 representative of the degree of carbonate dissolution, were significantly lower than
333 during their preceding counterparts (Fig. 2). In other words, the degree of carbonate
334 dissolution associated with the shoaling of the calcite compensation depth (CCD) and
335 lysocline appears to be less severe than during the first pulses. In this respect it is
336 worth noting that H2 and I2 also behave differently from the “larger” events in terms
337 of biotic disruption. During PETM, ETM2 and I1, rates of variability in planktonic
338 communities indicate that the biotic response was proportional to the magnitude of
339 carbon injections, and biotic disruption linearly declined along with the decreasing
340 size of CIEs (Gibbs et al., 2012; Jennions et al., 2015). However, H2 and I2 do not
341 show evidence of above-background variance, suggesting that during these events the
342 system apparently failed to cross the environmental “threshold” necessary to generate
343 a detectable marine biotic disruption (D’haenens et al., 2012; Gibbs et al., 2012). This
344 all suggests that a change in the climate feedbacks and/or an incomplete recovery of
345 the buffering capacity of the ocean system after the first perturbation could have
346 played a significant role in amplifying the temperature response during the secondary
347 pulse. On the other hand, we cannot dismiss the possibility that local circulation
348 changes and/or partial dissolution slightly altered the anomalies in $\delta^{18}\text{O}$ and $\delta^{13}\text{C}$
349 during H2 and I2 at Walvis Ridge. Further research is hence needed to ratify the
350 (global) significance of this finding.

351

352 5.3 Thresholds and orbital pacing

353 The transition towards the EECO is marked by a general decrease of both benthic
354 carbon and oxygen isotopic values of $\sim 0.3\text{‰}$ at Site 1263, indicative of both long-

Lauretano, V. (Vittoria) 16/9/2015 16:06

Deleted: was

Lauretano, V. (Vittoria) 16/9/2015 16:06

Deleted: been

Lauretano, V. (Vittoria) 16/9/2015 16:10

Deleted: the

Lauretano, V. (Vittoria) 16/9/2015 16:12

Deleted: te

359 term warming and progressive oxidation of organic matter releasing CO₂ into the
360 ocean-atmosphere system. It has been theorized that the timing and magnitude of the
361 hyperthermals would respond to the crossing of a thermal threshold, more frequently
362 reached in phases of orbital-driven temperature increase (Lourens et al., 2005; Lunt et
363 al., 2011). In addition, the carbon reservoir or capacitor (Dickens, 2003), regardless of
364 its nature and as a result of the long-term temperature increase from the late
365 Paleocene, to the early Eocene, would be largely depleted by the peak of the EECO,
366 leading to an interval free of hyperthermals. In turn, a series of orbitally paced global
367 warming events of decreasing frequency and increased size are expected to occur
368 during the post-EECO cooling phase when the carbon reservoir would have been
369 progressive refilled (e.g., Kirtland Turner et al., 2014). This hypothesis has been
370 questioned with data from a composite bulk stable isotope record of Site 1258
371 showing that a series of negative stable isotope excursions continued throughout the
372 EECO. This evidence suggests that episodes of carbon release persisted during the
373 peak of warmth and the onset of the cooling trend (Kirtland Turner et al., 2014).
374 Kirtland Turner and co-authors (2014) suggest that the mechanisms operating in the
375 early Eocene climate were not necessarily exceptional but actually similar to those
376 invoked for the Oligocene and Miocene when cyclic variations in the carbon cycle
377 were also clearly paced by orbital forcing, particularly in the eccentricity bands
378 (Holbourn et al., 2007; Pälike et al., 2006; Zachos et al., 2001b). Although the carbon
379 and oxygen isotope records of the Oligocene-Miocene and early Eocene are certainly
380 paced by eccentricity, their appearance in terms of punctuation are clearly different.
381 In particular, a relatively sudden release (storage) of large amounts of light carbon
382 (e.g. methane hydrates) into the ocean-atmosphere system seems the only way to
383 explain the unusual magnitude of the CIEs recorded at Walvis Ridge given the
384 rate/magnitude of warming, as well as carbonate dissolution and changes in benthic
385 assemblages associated with those events (Jennions et al., 2015; Stap et al., 2009).

386

387 **5.4 Site 1263 vs. Site 1262**

388 Comparison between the benthic $\delta^{13}\text{C}$ and $\delta^{18}\text{O}$ records of Sites 1263 and 1262
389 reveals an almost identical pattern, although $\delta^{18}\text{O}$ values of Site 1263 are consistently
390 $\sim 0.2\text{‰}$ heavier than those of Site 1262 (Fig. 3 and 4). A similar (reversed) pattern has
391 been previously observed by Stap et al. (2009) in the case of ETM2, and attributed to

Lauretano, V. (Vittoria) 16/9/2015 16:28

Deleted: between the

Lauretano, V. (Vittoria) 16/9/2015 16:27

Deleted:

Lauretano, V. (Vittoria) 16/9/2015 16:28

Deleted: -

Lauretano, V. (Vittoria) 16/9/2015 16:31

Deleted: ocean

Lauretano, V. (Vittoria) 16/9/2015 16:31

Deleted: the

397 differential dissolution from the shallowest to the deepest site. Conversely, selective
398 dissolution seems unlikely to justify the persistent offset in $\delta^{18}\text{O}$ values observed
399 throughout the new post-ETM2 record presented herein. We posit that this offset may
400 be linked to a different average isotopic composition of the water masses at those
401 sites. Accordingly, the intermediate water masses reaching Site 1263 were more ^{18}O -
402 enriched than the deeper waters at Site 1262. The existence of a discrete intermediate
403 water body in the early Eocene South Atlantic is supported by recent benthic
404 foraminiferal assemblage, sedimentological evidence and Earth system modeling data
405 across ETM2, which suggests that warming in the intermediate waters bathing Site
406 1263 led to differential patterns in sedimentary and ecological data between this site
407 and the deeper Site 1262 (Jennions et al., 2015).

408 **6 Conclusions**

409 New high-resolution benthic stable isotope records from ODP Sites 1262 and 1263
410 provide a detailed framework to explore the (transient) nature of early Eocene
411 hyperthermal events during the onset of the EECO. Our results further confirm the
412 link between large-scale carbon release and climate response to orbital forcing, in
413 particular to short- and long- eccentricity cycles. The transition towards the EECO is
414 marked by a general decrease of both benthic carbon and oxygen isotopic values of
415 $\sim 0.3\%$ at Site 1263, indicative of both long-term warming and progressive oxidation
416 of organic matter releasing CO_2 into the ocean-atmosphere system. Consistent
417 covariance between benthic carbon and oxygen isotopes demonstrates that global
418 temperatures and changes in the exogenic carbon pool were similarly coupled during
419 each of the studied hyperthermal events. In this regard, we found that the second
420 pulses of the paired hyperthermal events (i.e. H2 and I2) point to a slightly different
421 behavior. Whether this implies a larger role for a carbon reservoir characterized by a
422 heavier isotopic signature remains debatable and, hence, allows for further
423 consideration of other operational processes such as local circulation changes, partial
424 dissolution, or different climate feedbacks. Finally we found a constant offset in
425 oxygen isotopic values between Site 1263 and 1262, with the isotopic composition of
426 the shallower waters at Site 1263 consistently heavier than at Site 1262, suggesting
427 presence of a discrete water body at intermediate depths of the Walvis Ridge transect.

428 **Acknowledgements**

Lauretano, V. (Vittoria) 16/9/2015 16:57
Deleted: behaviour

430 | We are grateful to Gerald Dickens, Lee Kump and Philip Sexton for their constructive
431 | comments. We thank the International Ocean Discovery Program (IODP) for
432 | providing the samples used in this study. We also thank A. van Dijk at Utrecht
433 | University, and Dyke Andreasen and Chih-Ting Hsieh at UCSC for analytical
434 | support. This research was funded by NWO-ALW grant (project number 865.10.001)
435 | to L.J. Lourens. We thank F. Hilgen and H.A. Abels for providing valuable comments
436 | on the manuscript.

Vittoria 7/9/2015 22:45

Deleted: r

438 **References**

- 439 Abels, H. A., Clyde, W. C., Gingerich, P. D., Hilgen, F. J., Fricke, H. C., Bowen, G.
440 J. and Lourens, L. J.: Terrestrial carbon isotope excursions and biotic change during
441 Palaeogene hyperthermals, *Nat. Geosci.*, 5(5), 326–329, doi:10.1038/ngeo1427, 2012.
- 442 Abels, H. A., Lauretano, V., van Yperen, A., Hopman, T., Zachos, J. C., Lourens, L.
443 J., Gingerich, P. D., Bowen, G. J.: Carbon isotope excursions in paleosol carbonate
444 marking five early Eocene hyperthermals in the Bighorn Basin, Wyoming, *Clim. Past*
445 Discussion, <http://www.clim-past-discuss.net/11/1857/2015/cpd-11-1857-2015.html>.
- 446 Agnini, C., Macri, P., Backman, J., Brinkhuis, H., Fornaciari, E., Giusberti, L.,
447 Luciani, V., Rio, D., Sluijs, A. and Speranza, F.: An early Eocene carbon cycle
448 perturbation at ~52.5 Ma in the Southern Alps: Chronology and biotic response,
449 *Paleoceanography*, 24(2), doi:10.1029/2008PA001649, 2009.
- 450 Bemis, B. E., Spero, H. J., Bijma, J., and Lea, D. W.: Reevaluation of the oxygen
451 isotopic composition of planktonic foraminifera: Experimental results and revised
452 paleotemperature equations: *Paleoceanography*, v. 13, p. 150-160, 1998.
- 453 Bijl, P. K., Schouten, S., Sluijs, A., Reichert, G.-J., Zachos, J. C. and Brinkhuis, H.:
454 Early Palaeogene temperature evolution of the southwest Pacific Ocean., *Nature*,
455 461(7265), 776–9, doi:10.1038/nature08399, 2009.
- 456 Cramer, B. S., Wright, J. D., Kent, D. V and Aubry, M.-P.: Orbital climate forcing of
457 $\delta^{13}\text{C}$ excursions in the late Paleocene–early Eocene (chrons C24n–C25n),
458 *Paleoceanography*, 18(4), doi:10.1029/2003PA000909, 2003.
- 459 D’haenens, S., Bornemann, A., Stassen, P. and Speijer, R. P.: Multiple early Eocene
460 benthic foraminiferal assemblage and $\delta^{13}\text{C}$ fluctuations at DSDP Site 401 (Bay of
461 Biscay — NE Atlantic), *Mar. Micropaleontol.*, 88-89, 15–35,
462 doi:10.1016/j.marmicro.2012.02.006, 2012.
- 463 DeConto, R. M., Galeotti, S., Pagani, M., Tracy, D., Schaefer, K., Zhang, T., Pollard,
464 D. and Beerling, D. J.: Past extreme warming events linked to massive carbon release
465 from thawing permafrost., *Nature*, 484(7392), 87–91, doi:10.1038/nature10929, 2012.
- 466 Dickens, G. R.: Rethinking the global carbon cycle with a large, dynamic and
467 microbially mediated gas hydrate capacitor, *Earth Planet. Sci. Lett.*, 213(3-4), 169–
468 183, doi:10.1016/S0012-821X(03)00325-X, 2003.
- 469 Dickens, G.R., J.R. O’Neil, D.K. Rea, and R.M. Owen: Dissociation of oceanic
470 methane hydrate as a cause of the carbon isotope excursion at the end of the
471 Paleocene. *Paleoceanography* 10, 965-971, 1995.
- 472 Dinarès-Turell, J., Westerhold, T., Pujalte, V., Röhl, U. and Kroon, D.: Astronomical
473 calibration of the Danian stage (Early Paleocene) revisited: Settling chronologies of
474 sedimentary records across the Atlantic and Pacific Oceans, *Earth Planet. Sci. Lett.*,
475 405, 119–131, doi:10.1016/j.epsl.2014.08.027, 2014.

Lauretano, V. (Vittoria) 16/9/2015 17:09
Formatted: Font:Superscript

476 Galeotti, S., Krishnan, S., Pagani, M., Lanci, L., Gaudio, A., Zachos, J. C., Monechi,
477 S., Morelli, G. and Lourens, L. J.: Orbital chronology of Early Eocene hyperthermals
478 from the Contessa Road section, central Italy, *Earth Planet. Sci. Lett.*, 290(1-2), 192–
479 200, doi:10.1016/j.epsl.2009.12.021, 2010.

480 Gibbs, S. J., Bown, P. R., Murphy, B. H., Sluijs, A., Edgar, K. M., Pälike, H., Bolton,
481 C. T. and Zachos, J. C.: Scaled biotic disruption during early Eocene global warming
482 events, *Biogeosciences*, 9(11), 4679–4688, doi:10.5194/bg-9-4679-2012, 2012.

483 Hilgen, F. J., Abels, H. A., Kuiper, K. F., Lourens, L. J. and Wolthers, M.: Towards a
484 stable astronomical time scale for the Paleocene: Aligning Shatsky Rise with the
485 Zumaia – Walvis Ridge ODP Site 1262 composite, *Newsletters Stratigr.*, 48(1), 91–
486 110, doi:10.1127/nos/2014/0054, 2015.

487 Hilgen, F. J., Kuiper, K. F. and Lourens, L. J.: Evaluation of the astronomical time
488 scale for the Paleocene and earliest Eocene, *Earth Planet. Sci. Lett.*, 300(1-2), 139–
489 151, doi:10.1016/j.epsl.2010.09.044, 2010.

490 Holbourn, A., Kuhnt, W., Schulz, M., Flores, J-A. and Andersen, N.: Orbitally-paced
491 | climate evolution during the middle Miocene “Monterey” carbon isotope excursion,
492 *Earth Planet. Sci. Lett.* 261, 534–550, 2007.

493 Hönisch, B., Ridgwell, A., Schmidt, D. N., Thomas, E., Gibbs, S. J., Sluijs, A., Zeebe,
494 R., Kump, L., Martindale, R. C., Greene, S. E., Kiessling, W., Ries, J., Zachos, J. C.,
495 Royer, D. L., Barker, S., Marchitto, T. M., Moyer, R., Pelejero, C., Ziveri, P., Foster,
496 G. L. and Williams, B.: The geological record of ocean acidification, *Science*,
497 335(6072), 1058–63, doi:10.1126/science.1208277, 2012.

498 Hut, G.,: Consultants group meeting on stable isotope reference samples for
499 geochemical and hydrological investigations: Vienna, Austria, Report to Director
500 General of the Institute of Atomic Energy Agency, 42, 1987.

501 Jennions, S. M., Thomas, E., Schmidt, D. N., Lunt, D., and Ridgwell, A.: Changes in
502 benthic ecosystems and ocean circulation in the Southeast Atlantic across Eocene
503 Thermal Maximum 2, *Paleoceanography*, 30, doi:10.1002/2015PA002821, 2015.

504 Kennett, J. P. and Stott, L. D.: Abrupt deep-sea warming, palaeoceanographic
505 changes and benthic extinctions at the end of the Palaeocene, *Nature*, 353(6341), 225–
506 229, doi:10.1038/353225a0, 1991.

507 Kirtland Turner, S., Sexton, P. F., Charles, C. D. and Norris, R. D.: Persistence of
508 carbon release events through the peak of early Eocene global warmth, *Nat. Geosci.*,
509 12(9), 1–17, doi:10.1038/ngeo2240, 2014.

510 Kuiper, K. F., Deino, a, Hilgen, F. J., Krijgsman, W., Renne, P. R. and Wijbrans, J.
511 R.: Synchronizing rock clocks of Earth history., *Science*, 320(5875), 500–4,
512 doi:10.1126/science.1154339, 2008.

- 513 Kurtz, A. C., Kump, L. R., Arthur, M. A., Zachos, J. C. and Paytan, A.: Early
514 Cenozoic decoupling of the global carbon and sulfur cycles, *Paleoceanography*, 18(4),
515 doi:10.1029/2003PA000908, 2003.
- 516 Laskar, J., Fienga, A., Gastineau, M., and Manche, H.: La2010: A new orbital
517 solution for the long term motion of the Earth: *Astron. Astrophys.*, Volume 532, A89,
518 2011.
- 519 | Liebrand, D., Lourens, L. J., Hodell, D. A., De Boer, B., Van De Wal, R. S. W. and
520 Pälike, H.: Antarctic ice sheet and oceanographic response to eccentricity forcing
521 during the early Miocene, *Clim. Past*, 7(3), 869–880, doi:10.5194/cp-7-869-2011,
522 2011.
- 523 Littler, K., Röhl, U., Westerhold, T. and Zachos, J. C.: A high-resolution benthic
524 stable-isotope record for the South Atlantic: Implications for orbital-scale changes in
525 Late Paleocene-Early Eocene climate and carbon cycling, *Earth Planet. Sci. Lett.*,
526 401, 18–30, doi:10.1016/j.epsl.2014.05.054, 2014.
- 527 Lourens, L. J., Sluijs, A., Kroon, D., Zachos, J. C., Thomas, E., Röhl, U., Bowles, J.
528 and Raffi, I.: Astronomical pacing of late Palaeocene to early Eocene global warming
529 events., *Nature*, 435(7045), 1083–1087, doi:10.1038/nature03814, 2005.
- 530 Lunt, D. J., Valdes, P. J., Jones, T. D., Ridgwell, A., Haywood, A. M., Schmidt, D.
531 | N., Marsh, R. and Maslin, M.: CO₂-driven ocean circulation changes as an amplifier
532 of Paleocene-Eocene thermal maximum hydrate destabilization, *Geology*, 38(10),
533 875–878, doi:10.1130/G31184.1, 2010.
- 534 Lunt, D. J., Ridgwell, A., Sluijs, A., Zachos, J. C., Hunter, S. and Haywood, A.: A
535 model for orbital pacing of methane hydrate destabilization during the Palaeogene,
536 *Nat. Geosci.*, 4(11), 775–778, doi:10.1038/ngeo1266, 2011.
- 537 | McInerney, F. A. and Wing, S. L.: The Paleocene-Eocene Thermal Maximum: A
538 Perturbation of Carbon Cycle, Climate, and Biosphere with Implications for the
539 Future, *Annu. Rev. Earth Planet. Sci.*, 39(1), 489–516, doi:10.1146/annurev-earth-
540 040610-133431, 2011.
- 541 Nicolo, M. J., Dickens, G. R., Hollis, C. J. and Zachos, J. C.: Multiple early Eocene
542 hyperthermals: Their sedimentary expression on the New Zealand continental margin
543 and in the deep sea, *Geology*, 35(8), 699, doi:10.1130/G23648A.1, 2007.
- 544 Paillard, D., Labeyrie, L., Yiou, P.: Macintosh program performs time-series analysis.
545 *Eos Trans. AGU* 77, 379, 1996.
- 546 | Pälike, H., Norris, R. D., Herrle, J. O., Wilson, P. A., Coxall, H. K., Lear, C. H.,
547 Shackleton, N.J., Tripathi, A.K., Wade, B.S.: The heart-beat of the Oligocene climate
548 system, *Science* 314, 1894–1998, 2006.
- 549 Renne, P. R., Deino, A. L., Hilgen, F. J., Kuiper, K. F., Mark, D. F., Mitchell, W. S.,
550 Morgan, L. E., Mundil, R. and Smit, J.: Time scales of critical events around the

Lauretano, V. (Vittoria) 16/9/2015 17:08
Deleted: a

Lauretano, V. (Vittoria) 16/9/2015 17:32
Formatted: Font:Subscript

Lauretano, V. (Vittoria) 16/9/2015 17:33
Deleted: a

- 553 | Cretaceous-Paleogene boundary. *Science*, 339(6120), 684–7,
554 | doi:10.1126/science.1230492, 2013.
- 555 | Röhl, U., Westerhold, T., Monechi, S., Thomas, E., Zachos, J. C., Donner, B., 2005.
556 | The Third and Final Early Eocene Thermal Maximum: Characteristics, Timing and
557 | Mechanisms of the ‘X’ Event, GSA Annual Meeting 37. Geological Society of
558 | America, Salt Lake City, USA. 264 pp
- 559 | Sexton, P. F., Norris, R. D., Wilson, P. A., Pälike, H., Westerhold, T., Röhl, U.,
560 | Bolton, C. T. and Gibbs, S.: Eocene global warming events driven by ventilation of
561 | oceanic dissolved organic carbon, *Nature*, 471(7338), 349–352,
562 | doi:10.1038/nature09826, 2011.
- 563 | Shackleton, N. J., M. A. Hall, and A. Boersma: Oxygen and carbon isotope data from
564 | Leg-74 foraminifers, Initial Rep. Deep Sea Drill. Project, 74, 599–612, 1984.
- 565 | Shackleton, N. J., and Hall, M. A: The late Miocene stable isotope record, Site 926,
566 | Proc. Ocean Drill. Program Sci. Results, 154, 367–373. doi:
567 | 10.2973/odp.proc.sr.154.119.1997
- 568 | Slotnick, B. S., Dickens, G. R., Nicolo, M. J., Hollis, C. J., Crampton, J. S., Zachos, J.
569 | C. and Sluijs, A.: Large-Amplitude Variations in Carbon Cycling and Terrestrial
570 | Weathering during the Latest Paleocene and Earliest Eocene: The Record at Mead
571 | Stream, New Zealand, *J. Geol.*, 120(5), 487–505, doi:10.1086/666743, 2012.
- 572 | Sluijs, A., Brinkhuis, H., Schouten, S., Bohaty, S. M., John, C. M., Zachos, J. C.,
573 | Reichart, G.-J., Sinninghe Damsté, J. S., Crouch, E. M. and Dickens, G. R.:
574 | Environmental precursors to rapid light carbon injection at the Palaeocene/Eocene
575 | boundary., *Nature*, 450(7173), 1218–21, doi:10.1038/nature06400, 2007.
- 576 | Stap, L., Lourens, L. J., Thomas, E., Sluijs, A., Bohaty, S. and Zachos, J. C.: High-
577 | resolution deep-sea carbon and oxygen isotope records of Eocene Thermal Maximum
578 | 2 and H2, *Geology*, 38(7), 607–610, doi:10.1130/G30777.1, 2010.
- 579 | Stap, L., Sluijs, A., Thomas, E. and Lourens, L. J.: Patterns and magnitude of deep
580 | sea carbonate dissolution during Eocene Thermal Maximum 2 and H2, Walvis Ridge,
581 | southeastern Atlantic Ocean, *Paleoceanography*, 24(1), doi:10.1029/2008PA001655,
582 | 2009.
- 583 | Thomas, E. and Shackleton, N. J.: The Paleocene-Eocene benthic foraminiferal
584 | extinction and stable isotope anomalies, *Geol. Soc. London, Spec. Publ.*, 101(1), 401–
585 | 441, doi:10.1144/GSL.SP.1996.101.01.20, 1996.
- 586 | Westerhold, T. and Röhl, U.: High resolution cyclostratigraphy of the early Eocene –
587 | new insights into the origin of the Cenozoic cooling trend, *Clim. Past Discuss.*, 5(1),
588 | 495–534, 2009.
- 589 | Westerhold, T., Röhl, U., Laskar, J., Raffi, I., Bowles, J., Lourens, L. J. and Zachos, J.
590 | C.: On the duration of magnetochrons C24r and C25n and the timing of early Eocene
591 | global warming events: Implications from the Ocean Drilling Program Leg 208

Lauretano, V. (Vittoria) 16/9/2015 17:33

Deleted: .

Lauretano, V. (Vittoria) 16/9/2015 17:34

Formatted: Font:German

Lauretano, V. (Vittoria) 16/9/2015 17:34

Deleted: a

- 594 Walvis Ridge depth transect, *Paleoceanography*, 22(2), doi:10.1029/2006PA001322,
595 2007.
- 596 Westerhold, T., Röhl, U., Raffi, I., Fornaciari, E., Monechi, S., Reale, V., Bowles, J.
597 and Evans, H. F.: Astronomical calibration of the Paleocene time, *Palaeogeogr.*
598 *Palaeoclimatol. Palaeoecol.*, 257(4), 377–403, doi:10.1016/j.palaeo.2007.09.016,
599 2008.
- 600 Zachos, J. C., Pagani, M., Sloan, L., Thomas, E. and Billups, K.: Trends, rhythms,
601 and aberrations in global climate 65 Ma to present., *Science*, 292(5517), 686–693,
602 2001a.
- 603 Zachos, J. C., Shackleton, N. J., Revenaugh, J. S., Pälike, H., and Flower, B. P.,
604 Periodic and non-periodic climate response to orbital forcing across the Oligocene-
605 Miocene boundary. *Science*. 292, 274-277, 2001b
- 606 Zachos, J. C., Kroon, D. and Blum, P.: ODP Leg 208: The early Cenozoic extreme
607 climates transect along Walvis Ridge, *Proceedings of the Ocean Drilling Program*
608 *Initial Reports*, 208, 2004.
- 609 Zachos, J. C., Röhl, U., Schellenberg, S. A., Sluijs, A., Hodell, D. A., Kelly, D. C.,
610 Thomas, E., Nicolo, M., Raffi, I., Lourens, L. J., McCarren, H., and Kroon, D.: Rapid
611 acidification of the ocean during the Paleocene-Eocene thermal maximum.: *Science*
612 (New York, N.Y.), v. 308, no. 5728, p. 1611–5, doi: 10.1126/science.1109004, 2005.
- 613 Zachos, J. C., Dickens, G. R. and Zeebe, R. E.: An early Cenozoic perspective on
614 greenhouse warming and carbon-cycle dynamics., *Nature*, 451(7176), 279–283,
615 doi:10.1038/nature06588, 2008.
- 616 Zachos, J. C., McCarren, H., Murphy, B., Röhl, U. and Westerhold, T.: Tempo and
617 scale of late Paleocene and early Eocene carbon isotope cycles: Implications for the
618 origin of hyperthermals, *Earth Planet. Sci. Lett.*, 299(1-2), 242–249,
619 doi:10.1016/j.epsl.2010.09.004, 2010.
- 620 Zeebe, R. E. and Zachos, J. C.: Long-term legacy of massive carbon input to the Earth
621 system: Anthropocene versus Eocene., *Philos. Trans. A. Math. Phys. Eng. Sci.*,
622 371(2001), 2013.
- 623

Lauretano, V. (Vittoria) 16/9/2015 11:57

Deleted:

625 | TABLE 1: Age-depth tie points based on the tuning of the filtered 3-m period extracted from
 626 | the color reflectance record of Site 1262 and the long-eccentricity cycle extracted from the
 627 | Laskar solution La2010d (Laskar et al., 2011).

628

Site 1262 3-m period filter	Long-eccentricity cycle (kyrs)	Long-eccentricity cycle (kyrs)
	Laskar 2010d (Option 1)	Laskar 2010d (Option 2)
102.750	51800	52206
104.231	52003	52410
105.711	52206	52614
107.167	52410	52816
108.648	52614	53017
110.129	52816	53216
111.635	53017	53415
113.193	53216	53615
114.750	53415	53815
116.359	53615	54016
117.865	53815	54218

629

- Lauretano, V. (Vittoria) 16/9/2015 17:37
Deleted: 3
- Lauretano, V. (Vittoria) 16/9/2015 17:37
Deleted: -
- Lauretano, V. (Vittoria) 16/9/2015 17:38
Deleted: Site 1262
- Lauretano, V. (Vittoria) 16/9/2015 17:39
Deleted: long
- Lauretano, V. (Vittoria) 16/9/2015 17:39
Deleted: Long
- Lauretano, V. (Vittoria) 16/9/2015 17:39
Deleted: Long

636
637

TABLE 2: Tie points between ODP Site 1263 and Site 1262 based on color reflectance records and interpolated ages obtained from the astronomically tuned age model.

Lauretano, V. (Vittoria) 16/9/2015 17:39
Deleted: Color reflectance t
Lauretano, V. (Vittoria) 16/9/2015 17:39
Deleted: from

Samples	Site 1263 Depth (mbsf)	Site 1263 Depth (mcd)	Samples	Site 1262 Depth (mbsf)	Site 1262 Depth (mcd)	Interpolated Age (Ma)	
						Option 1	Option 2
1263A-26H-4, 147.5	228.575	265.425	1262B-11H-4, 137.5	92.275	101.855	51.610	52.014
1263A-26H-5, 50	229.1	265.95	1262B-11H-5, 42.5	92.825	102.405	51.727	52.132
1263A-26H-5, 90	229.5	266.35	1262B-11H-5, 102.5	93.425	103.005	51.835	52.241
1263A-26H-5, 115	229.75	266.6	1262B-11H-5, 137.5	93.775	103.355	51.883	52.289
1263A-26H-6, 147.5	231.575	268.425	1262B-11H-6, 45	94.35	103.93	51.962	52.369
1263A-26H-7, 30	231.9	268.75	1262A-10H-2, 120	88.2	104.31	52.014	52.421
1263B-22H-5, 100	230.9	269.23	1262A-10H-2, 145	88.45	104.56	52.048	52.455
1263B-22H-5, 125	231.15	269.48	1262A-10H-3, 20	88.7	104.81	52.082	52.490
1263B-22H-6, 142.5	232.825	271.155	1262A-10H-3, 60	89.1	105.21	52.137	52.545
1263B-22H-7, 45	233.35	271.68	1262A-10H-3, 87.5	89.375	105.485	52.175	52.583
1263A-27H-1, 65	232.75	272.78	1262A-10H-4, 2.5	90.025	106.135	52.265	52.673
1263A-27H-2, 7.5	233.675	273.705	1262A-10H-4, 27.5	90.275	106.385	52.300	52.707
1263A-27H-2, 17.5	233.775	273.805	1262A-10H-4, 37.5	90.375	106.485	52.314	52.721
1263A-27H-2, 25	233.85	273.88	1262A-10H-4, 45	90.45	106.56	52.325	52.732
1263A-27H-2, 125	234.85	274.88	1262A-10H-4, 77.5	90.775	106.885	52.370	52.777
1263A-27H-2, 145	235.05	275.08	1262B-12H-1, 70	96.6	107.24	52.420	52.826
1263A-27H-3, 40	235.5	275.53	1262B-12H-1, 85	96.75	107.39	52.441	52.846
1263A-27H-3, 67.5	235.775	275.805	1262B-12H-1, 100	96.9	107.54	52.461	52.867
1263A-27H-3, 100	236.1	276.13	1262B-12H-1, 110	97	107.64	52.475	52.880
1263A-27H-3, 135	236.45	276.48	1262B-12H-1, 120	97.1	107.74	52.489	52.894
1263A-27H-4, 77.5	237.375	277.405	1262B-12H-2, 5	97.45	108.09	52.537	52.941
1263A-27H-4, 100	237.6	277.63	1262B-12H-2, 22.5	97.625	108.265	52.561	52.965
1263A-27H-4, 137.5	237.975	278.005	1262B-12H-2, 60	98	108.64	52.613	53.016
1263A-27H-5, 70	238.8	278.83	1262B-12H-2, 110	98.5	109.14	52.681	53.083
1263C-9H-4, 105	240.45	280.24	1262B-12H-2, 135	98.75	109.39	52.715	53.117
1263C-9H-5, 15	241.05	280.84	1262B-12H-3, 12.5	99.025	109.665	52.753	53.154
1263C-9H-5, 100	241.9	281.69	1262B-12H-3, 40	99.3	109.94	52.790	53.191
1263C-9H-6, 2.5	242.425	282.215	1262B-12H-3, 57.5	99.475	110.115	52.814	53.214
1263C-9H-6, 15	242.55	282.34	1262B-12H-3, 65	99.55	110.19	52.824	53.224
1263C-9H-6, 32.5	242.725	282.515	1262B-12H-3, 85	99.75	110.39	52.851	53.251
1263C-9H-6, 82.5	243.225	283.015	1262B-12H-4, 10	100.5	111.14	52.951	53.350
1263A-28H-1, 40	242	284.52	1262B-12H-4, 65	101.05	111.69	53.024	53.422
1263A-28H-1, 95	242.55	285.07	1262B-12H-4, 122.5	101.625	112.265	53.097	53.496
1263A-28H-1, 115	242.75	285.27	1262A-11H-1, 137.5	96.375	112.425	53.118	53.516
1263A-28H-2, 40	243.5	286.02	1262A-11H-2, 2.5	96.525	112.575	53.137	53.536
1263A-28H-2, 70	243.8	286.32	1262A-11H-2, 12.5	96.625	112.675	53.150	53.549
1263A-28H-2, 107.5	244.175	286.695	1262A-11H-2, 50	97	113.05	53.198	53.597
1263A-28H-3, 5	244.65	287.17	1262A-11H-2, 67.5	97.175	113.225	53.220	53.619
1263A-28H-3, 27.5	244.875	287.395	1262A-11H-2, 80	97.3	113.35	53.236	53.635
1263A-28H-3, 32.5	244.925	287.445	1262A-11H-2, 85	97.35	113.4	53.243	53.642

Lauretano, V. (Vittoria) 16/9/2015 17:40
Deleted:
Lauretano, V. (Vittoria) 16/9/2015 17:40
Deleted:

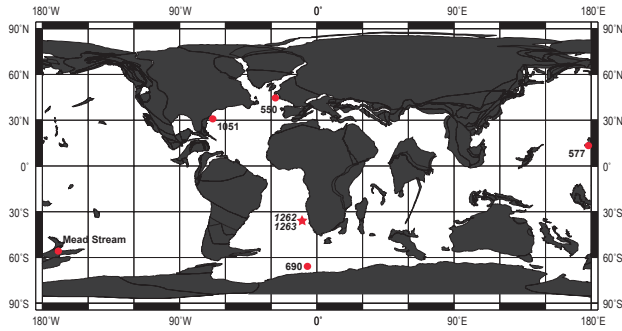
1263A-28H-3, 65	245.25	287.77	1262A-11H-2, 97.5	97.475	113.525	53.258	53.658
1263A-28H-3, 70	245.3	287.82	1262A-11H-2, 105	97.55	113.6	53.268	53.667
1263B-24H-2, 147.5	245.875	288.165	1262A-11H-2, 132.5	97.825	113.875	53.303	53.703
1263B-24H-3, 67.5	246.575	288.865	1262A-11H-2, 147.5	97.975	114.025	53.322	53.722
1263B-24H-4, 135	248.75	291.04	1262A-11H-3, 95	98.95	115	53.446	53.846
1263B-24H-5, 47.5	249.375	291.665	1262A-11H-3, 145	99.45	115.5	53.508	53.909
1263B-24H-6, 20	250.6	292.89	1262A-11H-4, 52.5	100.025	116.075	53.580	53.981
1263C-10H-5, 65	251.05	292.93	1262A-11H-4, 57.5	100.075	116.125	53.586	53.987
1263C-10H-5, 82.5	251.225	293.105	1262A-11H-4, 72.5	100.225	116.275	53.605	54.006
1263C-10H-5, 110	251.5	293.38	1262A-11H-4, 87.5	100.375	116.425	53.624	54.025
1263C-10H-7, 1	252.91	294.79	1262A-11H-4, 135	100.85	116.9	53.687	54.089
1263C-10H-7, 5	252.95	294.83	1262A-11H-5, 5	101.05	117.1	53.713	54.089
1263C-10H-7, 10	253	294.88	1262A-11H-5, 10	101.1	117.15	53.720	54.122

642

643 **FIGURES**

644 **Figure 1:** Paleogeographic reconstruction for the early Eocene (~54 Ma) showing the
645 position of Sites 1263 and 1262 (Walvis Ridge), (map provided by Ocean Drilling
646 Stratigraphic Network, ODSN;
647 <http://www.odsn.de/odsn/services/paleomap/paleomap.html>, modified). Also shown
648 the locations of ODP Sites 690 and 1051 and DSDP Sites 550 and 577 (Cramer et al.,
649 2003) and Mead Stream (Slotnick et al., 2012).

650

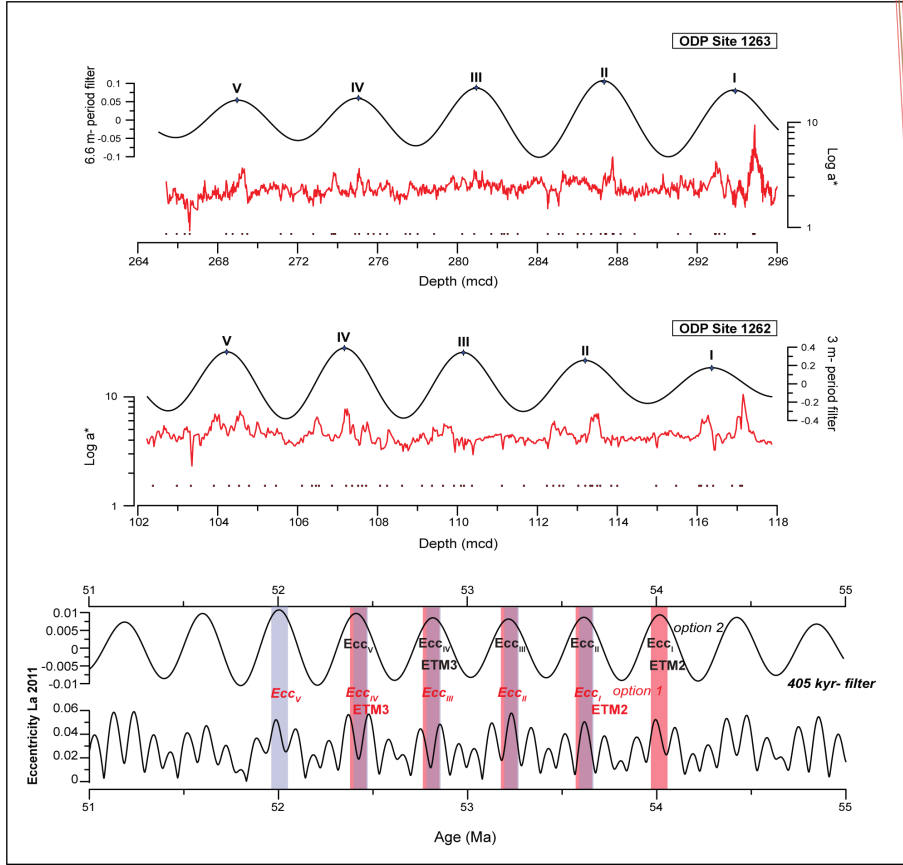


651

652

Lauretano, V. (Vittoria) 16/9/2015 17:41
Deleted: approximate

654 **Figure 2:** Floating orbitally tuned age model constructed using the red over green
 655 color ratio (a^*) record of ODP Sites 1262 (red line) and transferred to Site 1263 by
 656 using age-depth tie points between the sites (black dots, see Table 2). Two different
 657 tuning options are shown based on the ages proposed for the PETM by Westerhold et
 658 al. (2008).

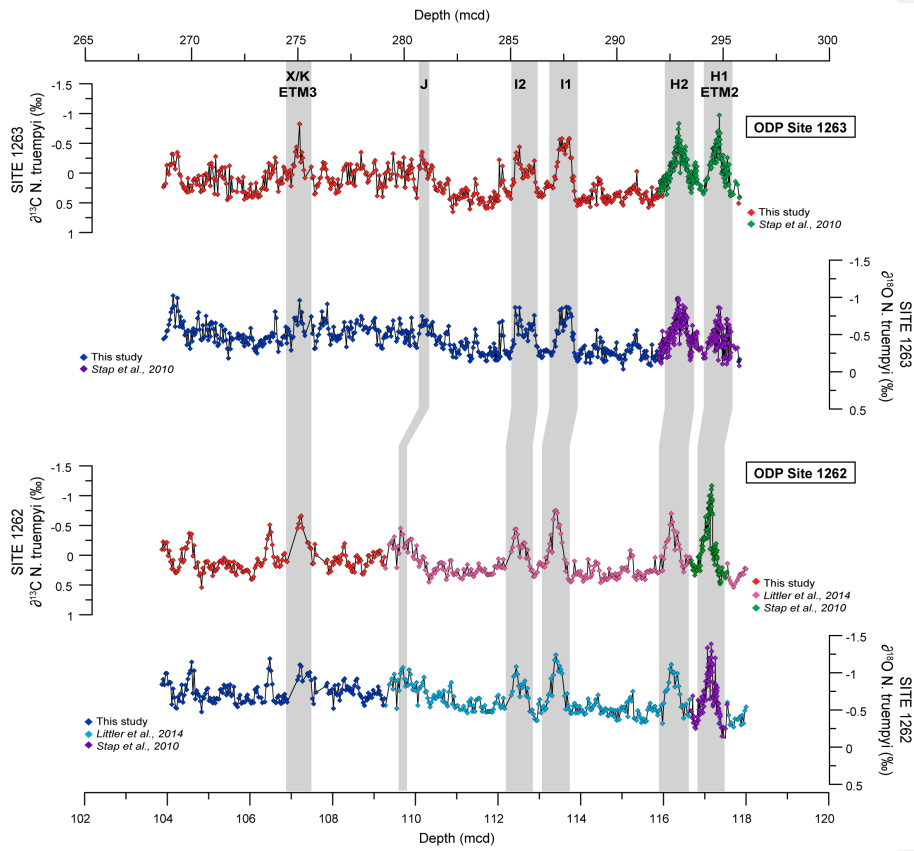


659
 660

- Lauretano, V. (Vittoria) 16/9/2015 17:48
- Deleted:** The f
- Lauretano, V. (Vittoria) 16/9/2015 17:48
- Deleted:** was
- Lauretano, V. (Vittoria) 16/9/2015 17:48
- Deleted:** based on
- Vittoria 17/9/2015 12:40
- Deleted:** 3
- Vittoria 17/9/2015 12:41
- Deleted:** 1262 (red line)
- Vittoria 17/9/2015 12:42
- Deleted:** .
- Lauretano, V. (Vittoria) 16/9/2015 17:53
- Moved down [1]:** (Westerhold et al., 2008)
- Lauretano, V. (Vittoria) 16/9/2015 17:46
- Deleted:** The extracted ~3-m period from Site 1262 was used to tune the record to the extracted 405-kyr eccentricity component of the La2010d orbital solution (Laskar et al., 2011), with maximum a^* values corresponding to maximum eccentricity values.
- Vittoria 17/9/2015 12:41
- Deleted:** Black dots represent
- Lauretano, V. (Vittoria) 16/9/2015 17:45
- Deleted:** Interpolated ages were transferred then to Site 1263 by using
- Lauretano, V. (Vittoria) 16/9/2015 17:49
- Deleted:** (black dots)
- Lauretano, V. (Vittoria) 16/9/2015 17:50
- Deleted:** . Uncertainties in dating proxies prevent an absolute age for this time interval, anchored to the lack of an absolute age for the PETM. Therefore, different tuning options are available within an 800 kyr window
- Lauretano, V. (Vittoria) 16/9/2015 17:53
- Deleted:** .
- Lauretano, V. (Vittoria) 16/9/2015 17:50
- Deleted:** possible options
- Lauretano, V. (Vittoria) 16/9/2015 17:53
- Moved (insertion) [1]**
- Lauretano, V. (Vittoria) 16/9/2015 17:57
- Deleted:** (
- Lauretano, V. (Vittoria) 16/9/2015 17:57
- Deleted:** ,
- Lauretano, V. (Vittoria) 16/9/2015 17:44
- Deleted:** .
- Vittoria 17/9/2015 13:47
- Deleted:** -

... [1]

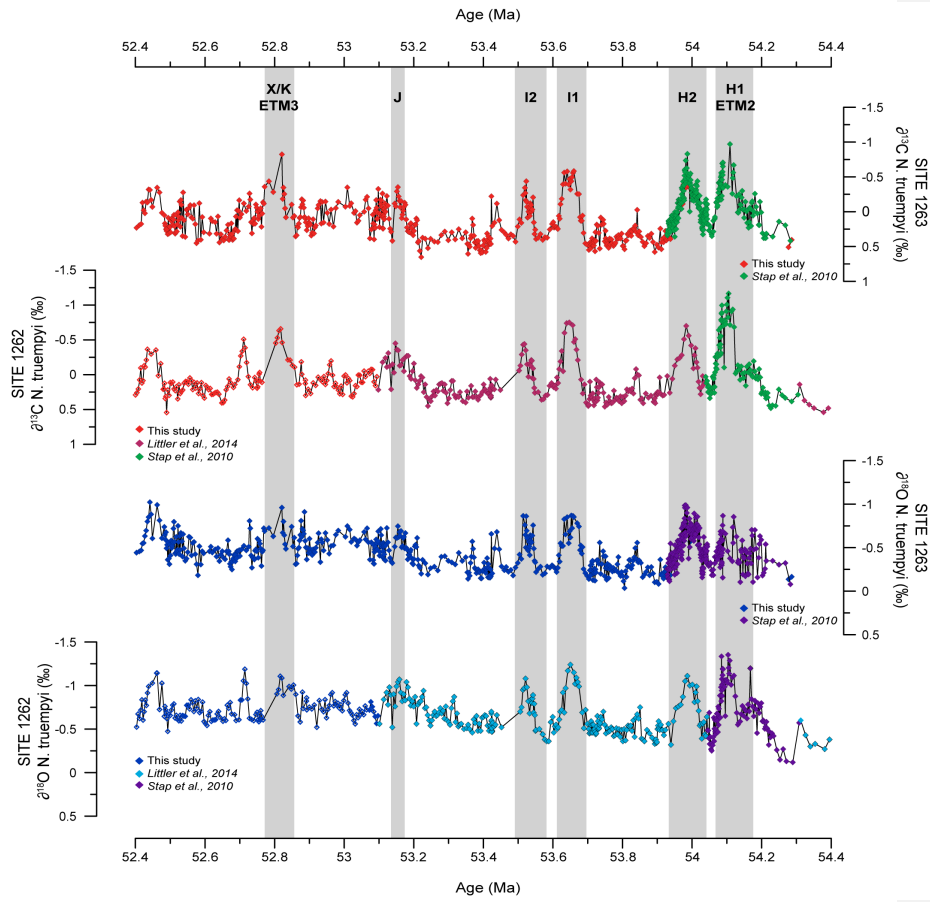
691 **Figure 3:** Benthic *N. truempyi* $\delta^{13}\text{C}$ and $\delta^{18}\text{O}$ records from Site 1263 and Site 1262,
692 plotted versus depth. Highlighted intervals represent the position of the early Eocene
693 hyperthermal events.



694

695

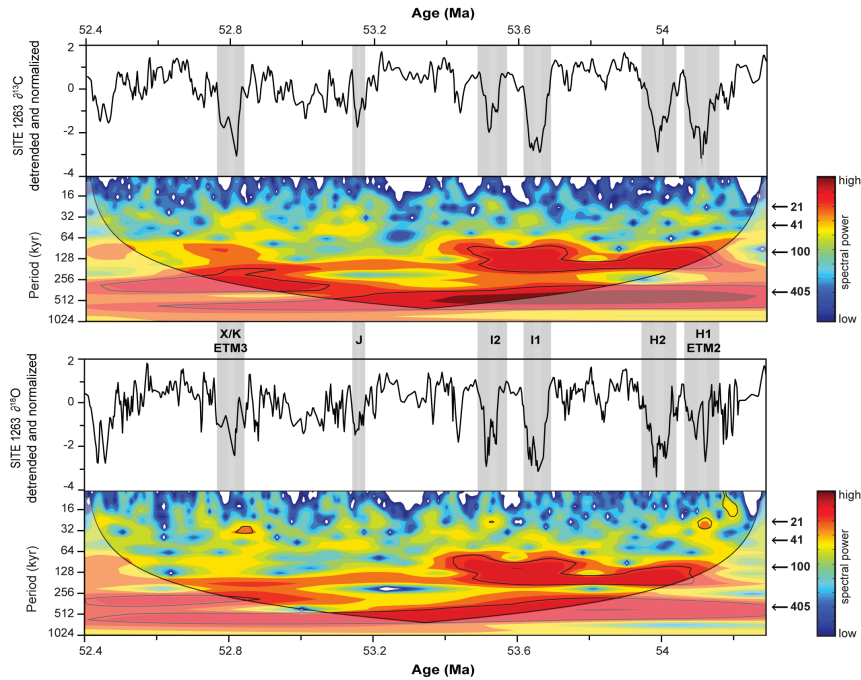
696 **Figure 4:** Benthic *N. truempyi* $\delta^{13}\text{C}$ and $\delta^{18}\text{O}$ records from Site 1263 and Site 1262,
 697 plotted versus Age (Ma), (starting from option 2 for the age of ETM2 by Westerhold
 698 et al., 2008). Highlighted intervals represent the position of the early Eocene
 699 hyperthermal events.



700

701

702 **Figure 5:** Evolutionary wavelet analyses for $\delta^{13}\text{C}$ and $\delta^{18}\text{O}$ were performed using a
 703 Morlet mother wavelet of an order of 6. Shaded areas represent 95% significance
 704 levels. Spectral power above the confidence level is concentrated at distinct
 705 frequencies, corresponding to the long 405-kyr and short eccentricity 100-kyr cycles.
 706 Highlighted intervals represent the position of the early Eocene hyperthermal events.



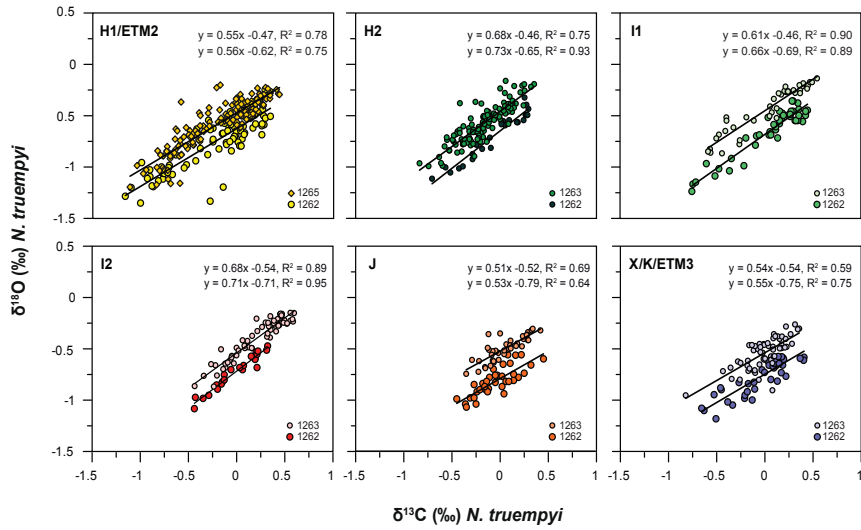
707

708

Lauretano, V. (Vittoria) 16/9/2015 18:00
 Deleted: The s
 Lauretano, V. (Vittoria) 16/9/2015 18:00
 Deleted: s
 Lauretano, V. (Vittoria) 16/9/2015 18:00
 Deleted: the

712 **Figure 6:** Relationship between the oxygen and carbon isotope values of *N. truempyi*
 713 during ETM2, H2, I1, I2, J and ETM3/X at Site 1263 and Site 1262. Note that,
 714 because of intense dissolution at Site 1263, ETM2 data were chosen from Site 1265
 715 (Stap et al., 2010). For all the events, throughout the entire event (onset+recovery
 716 phases), changes in the exogenic carbon pool are linearly related to warming. Linear
 717 regression equations refer to Site 1263 (top) and Site 1262 (bottom), respectively.

Lauretano, V. (Vittoria) 16/9/2015 18:01
 Deleted: Data for ETM2 and H2 from Stap et al. (2010) and for I1, I2 and J at Site 1262 from Littler et al. (2014).

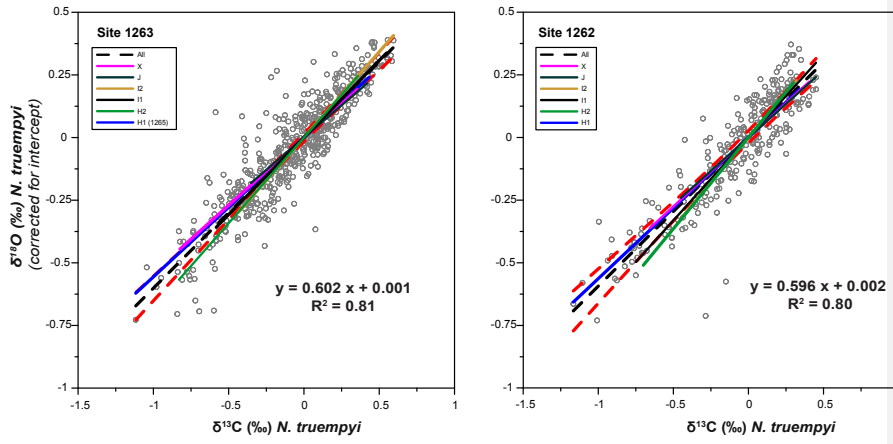


718

719

723 | **Figure 7:** Regression line between $\delta^{13}\text{C}$ and $\delta^{18}\text{O}$ for each event plotted together with
724 | the average slope (from all the events) at each site. The red dashed line indicates the
725 | 99% confidence interval.

Vittoria 17/9/2015 13:50
Deleted: Slope of the r
Vittoria 17/9/2015 13:50
Deleted: for



726